EUROPEAN LABORATORY FOR PARTICLE PHYSICS

CERN-PPE/97-06
10^{th} January 1997

Measurements of the b quark forward-backward asymmetry around the Z^0 peak using jet charge and vertex charge

The OPAL Collaboration

Abstract

The b quark forward-backward asymmetry has been measured using approximately four million hadronic Z^0 decays collected with the OPAL detector at LEP. Both jet charge and vertex charge were used to estimate whether the b quark was produced in the forward or backward thrust hemisphere. The measured values corrected to the hadron-level thrust axis are

$$\begin{aligned} A_{\rm FB}^{\rm b} &= 0.041 \pm 0.021 \pm 0.002 \qquad \sqrt{s} = 89.44 \text{ GeV} \\ A_{\rm FB}^{\rm b} &= 0.0994 \pm 0.0052 \pm 0.0044 \qquad \sqrt{s} = 91.21 \text{ GeV} \\ A_{\rm FB}^{\rm b} &= 0.145 \pm 0.017 \pm 0.007 \qquad \sqrt{s} = 92.91 \text{ GeV} \end{aligned}$$

where in each case the first error is statistical and the second systematic. Within the framework of the Standard Model these measurements correspond to an effective weak mixing angle of $\sin^2\theta_{\rm W}^{\rm eff,e} = 0.2308 \pm 0.0013$. The measurements are in agreement with the Standard Model and other measurements at LEP.

(Submitted to Z. Phys.)

The OPAL Collaboration

K. Ackerstaff[8], G. Alexander[23], J. Allison[16], N. Altekamp[5], K. Ametewee[25], K.J. Anderson[9], S. Anderson[12], S. Arcelli[2], S. Asai[24], D. Axen[29], G. Azuelos[18,a], A.H. Ball[17], E. Barberio[8], R.J. Barlow[16], R. Bartoldus[3], J.R. Batley[5], J. Bechtluft[14], C. Beeston[16], T. Behnke[8], A.N. Bell[1], K.W. Bell[20], G. Bella[23], S. Bentvelsen[8], P. Berlich[10], S. Bethke[14], O. Biebel[14], A. Biguzzi[5], S.D. Bird[16], V. Blobel[27], I.J. Bloodworth[1], J.E. Bloomer[1], M. Bobinski[10], P. Bock[11], H.M. Bosch[11], M. Boutemeur[34], B.T. Bouwens[12], S. Braibant[12], R.M. Brown[20], H.J. Burckhart[8], C. Burgard[8], R. Bürgin[10], P. Capiluppi[2], R.K. Carnegie[6], A.A. Carter[13], J.R. Carter[5], C.Y. Chang[17], D.G. Charlton[1,b], D. Chrisman[4], P.E.L. Clarke[15], I. Cohen[23], J.E. Conboy[15], O.C. Cooke[16], M. Cuffiani[2], S. Dado[22], C. Dallapiccola[17], G.M. Dallavalle[2], S. De Jong[12], L.A. del Pozo[4], K. Desch[3], M.S. Dixit[7], E. do Couto e Silva[12], M. Doucet[18], E. Duchovni[26], G. Duckeck[34], I.P. Duerdoth[16], D. Eatough[16], J.E.G. Edwards[16], P.G. Estabrooks[6], H.G. Evans[9], M. Evans[13], F. Fabbri[2], M. Fanti[2], P. Fath[11], A.A. Faust[30], F. Fiedler[27], M. Fierro[2], H.M. Fischer[3], R. Folman[26], D.G. Fong[17], M. Foucher[17], A. Fürtjes[8], P. Gagnon[7], A. Gaidot[21], J.W. Gary[4], J. Gascon[18], S.M. Gascon-Shotkin[17], N.I. Geddes[20], C. Geich-Gimbel[3], F.X. Gentit[21], T. Geralis[20], G. Giacomelli[2], P. Giacomelli[4], R. Giacomelli[2], V. Gibson[5], W.R. Gibson[13], D.M. Gingrich[30,a], D. Glenzinski[9], J. Goldberg[22], M.J. Goodrick[5], W. Gorn[4], C. Grandi[2], E. Gross[26], J. Grunhaus[23], M. Gruwé[8], C. Hajdu[32], G.G. Hanson[12], M. Hansroul[8], M. Hapke[13], C.K. Hargrove[7], P.A. Hart[9], C. Hartmann[3], M. Hauschild[8], C.M. Hawkes[5], R. Hawkings[27], R.J. Hemingway[6], M. Herndon[17], G. Herten[10], R.D. Heuer[8], M.D. Hildreth[8], J.C. Hill[5], S.J. Hillier[1], T. Hilse[10], P.R. Hobson[25], R.J. Homer[1], A.K. Honma[28,a], D. Horváth[32,c], R. Howard[29], R.E. Hughes-Jones[16], D.E. Hutchcroft[5], P. Igo-Kemenes[11], D.C. Imrie[25], M.R. Ingram[16], K. Ishii[24], A. Jawahery[17], P.W. Jeffreys[20], H. Jeremie[18], M. Jimack[1], A. Joly[18], C.R. Jones[5], G. Jones[16], M. Jones[6], R.W.L. Jones[8], U. Jost[11], P. Jovanovic[1], T.R. Junk[8], D. Karlen[6], K. Kawagoe[24], T. Kawamoto[24], R.K. Keeler[28], R.G. Kellogg[17], B.W. Kennedy[20], J. Kirk[29], S. Kluth[8], T. Kobayashi[24], M. Kobel[10], D.S. Koetke[6], T.P. Kokott[3], M. Kolrep[10], S. Komamiya[24], T. Kress[11], P. Krieger[6], J. von Krogh[11], P. Kyberd[13], G.D. Lafferty[16], H. Lafoux[21], R. Lahmann[17], W.P. Lai[19], D. Lanske[14], J. Lauber[15], S.R. Lautenschlager[31], J.G. Layter[4], D. Lazic[22], A.M. Lee[31], E. Lefebvre[18], D. Lellouch[26], J. Letts[12], L. Levinson[26], C. Lewis[15], S.L. Lloyd[13], F.K. Loebinger[16], G.D. Long[28], M.J. Losty[7], J. Ludwig[10], A. Macchiolo[2], A. Macpherson[30], A. Malik[21], M. Mannelli[8], S. Marcellini[2], C. Markus[3], A.J. Martin[13], J.P. Martin[18], G. Martinez[17], T. Mashimo[24], W. Matthews[25], P. Mättig[3], W.J. McDonald[30], J. McKenna[29], E.A. Mckigney[15], T.J. McMahon[1], A.I. McNab[13], R.A. McPherson[8], F. Meijers[8], S. Menke[3], F.S. Merritt[9], H. Mes[7], J. Meyer[27], A. Michelini[2], G. Mikenberg[26], D.J. Miller[15], R. Mir[26], W. Mohr[10], A. Montanari[2], T. Mori[24], M. Morii[24], U. Müller[3], K. Nagai[26], I. Nakamura[24], H.A. Neal[8], B. Nellen[3], B. Nijjhar[16], R. Nisius[8], S.W. O'Neale[1], F.G. Oakham[7], F. Odorici[2], H.O. Ogren[12], N.J. Oldershaw[16], T. Omori[24], M.J. Oreglia[9], S. Orito[24], J. Pálinkás[33,d], G. Pásztor[32], J.R. Pater[16], G.N. Patrick[20], J. Patt[10], M.J. Pearce[1], S. Petzold[27], P. Pfeifenschneider[14], J.E. Pilcher[9], J. Pinfold[30], D.E. Plane[8], P. Poffenberger[28], B. Poli[2], A. Posthaus[3], H. Przysiezniak[30], D.L. Rees[1], D. Rigby[1], S. Robertson[28], S.A. Robins[13], N. Rodning[30], J.M. Roney[28], A. Rooke[15], E. Ros[8], A.M. Rossi[2], M. Rosvick[28], P. Routenburg[30], Y. Rozen[22], K. Runge[10], O. Runolfsson[8], U. Ruppel[14], D.R. Rust[12], R. Rylko[25], K. Sachs[10], E.K.G. Sarkisyan[23], M. Sasaki[24], C. Sbarra[29], A.D. Schaile[34], O. Schaile[34], F. Scharf[3], P. Scharff-Hansen[8], P. Schenk[34], B. Schmitt[8], S. Schmitt[11], M. Schröder[8],

H.C. Schultz-Coulon[10], M. Schulz[8], M. Schumacher[3], P. Schütz[3], W.G. Scott[20], T.G. Shears[16], B.C. Shen[4], C.H. Shepherd-Themistocleous[8], P. Sherwood[15], G.P. Siroli[2], A. Sittler[27], A. Skillman[15], A. Skuja[17], A.M. Smith[8], T.J. Smith[28], G.A. Snow[17], R. Sobie[28], S. Söldner-Rembold[10], R.W. Springer[30], M. Sproston[20], A. Stahl[3], M. Steiert[11], K. Stephens[16], J. Steuerer[27], B. Stockhausen[3], D. Strom[19], P. Szymanski[20], R. Tafirout[18], S.D. Talbot[1], S. Tanaka[24], P. Taras[18], S. Tarem[22], M. Thiergen[10], M.A. Thomson[8], E. von Törne[3], S. Towers[6], I. Trigger[18], T. Tsukamoto[24], E. Tsur[23], A.S. Turcot[9], M.F. Turner-Watson[8], P. Utzat[11], R. Van Kooten[12], G. Vasseur[21], M. Verzocchi[10], P. Vikas[18], M. Vincter[28], E.H. Vokurka[16], F. Wäckerle[10], A. Wagner[27], C.P. Ward[5], D.R. Ward[5], J.J. Ward[15], P.M. Watkins[1], A.T. Watson[1], N.K. Watson[1], P.S. Wells[8], N. Wermes[3], J.S. White[28], B. Wilkens[10], G.W. Wilson[27], J.A. Wilson[1], G. Wolf[26], S. Wotton[5], T.R. Wyatt[16], S. Yamashita[24], G. Yekutieli[26], V. Zacek[18], D. Zer-Zion[8]

[1]School of Physics and Space Research, University of Birmingham, Birmingham B15 2TT, UK
[2]Dipartimento di Fisica dell' Università di Bologna and INFN, I-40126 Bologna, Italy
[3]Physikalisches Institut, Universität Bonn, D-53115 Bonn, Germany
[4]Department of Physics, University of California, Riverside CA 92521, USA
[5]Cavendish Laboratory, Cambridge CB3 0HE, UK
[6] Ottawa-Carleton Institute for Physics, Department of Physics, Carleton University, Ottawa, Ontario K1S 5B6, Canada
[7]Centre for Research in Particle Physics, Carleton University, Ottawa, Ontario K1S 5B6, Canada
[8]CERN, European Organisation for Particle Physics, CH-1211 Geneva 23, Switzerland
[9]Enrico Fermi Institute and Department of Physics, University of Chicago, Chicago IL 60637, USA
[10]Fakultät für Physik, Albert Ludwigs Universität, D-79104 Freiburg, Germany
[11]Physikalisches Institut, Universität Heidelberg, D-69120 Heidelberg, Germany
[12]Indiana University, Department of Physics, Swain Hall West 117, Bloomington IN 47405, USA
[13]Queen Mary and Westfield College, University of London, London E1 4NS, UK
[14]Technische Hochschule Aachen, III Physikalisches Institut, Sommerfeldstrasse 26-28, D-52056 Aachen, Germany
[15]University College London, London WC1E 6BT, UK
[16]Department of Physics, Schuster Laboratory, The University, Manchester M13 9PL, UK
[17]Department of Physics, University of Maryland, College Park, MD 20742, USA
[18]Laboratoire de Physique Nucléaire, Université de Montréal, Montréal, Quebec H3C 3J7, Canada
[19]University of Oregon, Department of Physics, Eugene OR 97403, USA
[20]Rutherford Appleton Laboratory, Chilton, Didcot, Oxfordshire OX11 0QX, UK
[21]CEA, DAPNIA/SPP, CE-Saclay, F-91191 Gif-sur-Yvette, France
[22]Department of Physics, Technion-Israel Institute of Technology, Haifa 32000, Israel
[23]Department of Physics and Astronomy, Tel Aviv University, Tel Aviv 69978, Israel
[24]International Centre for Elementary Particle Physics and Department of Physics, University of Tokyo, Tokyo 113, and Kobe University, Kobe 657, Japan
[25]Brunel University, Uxbridge, Middlesex UB8 3PH, UK
[26]Particle Physics Department, Weizmann Institute of Science, Rehovot 76100, Israel

[27]Universität Hamburg/DESY, II Institut für Experimental Physik, Notkestrasse 85, D-22607 Hamburg, Germany
[28]University of Victoria, Department of Physics, P O Box 3055, Victoria BC V8W 3P6, Canada
[29]University of British Columbia, Department of Physics, Vancouver BC V6T 1Z1, Canada
[30]University of Alberta, Department of Physics, Edmonton AB T6G 2J1, Canada
[31]Duke University, Dept of Physics, Durham, NC 27708-0305, USA
[32]Research Institute for Particle and Nuclear Physics, H-1525 Budapest, P O Box 49, Hungary
[33]Institute of Nuclear Research, H-4001 Debrecen, P O Box 51, Hungary
[34]Ludwigs-Maximilians-Universität München, Sektion Physik, Am Coulombwall 1, D-85748 Garching, Germany

[a] and at TRIUMF, Vancouver, Canada V6T 2A3
[b] and Royal Society University Research Fellow
[c] and Institute of Nuclear Research, Debrecen, Hungary
[d] and Department of Experimental Physics, Lajos Kossuth University, Debrecen, Hungary

1 Introduction

The differential cross-section for the production of fermion-antifermion pairs in e^+e^- annihilation can be expressed as

$$\frac{d\sigma}{d\cos\theta} \propto 1 + \cos^2\theta + \frac{8}{3} A_{FB} \cos\theta, \tag{1}$$

where θ is the angle between the directions of the outgoing fermion and incoming electron, and where mass and higher order terms have been neglected. The term A_{FB} is the forward-backward asymmetry, which is defined as:

$$A_{FB} = \frac{\int_0^{+1} (d\sigma/d\cos\theta)\, d\cos\theta - \int_{-1}^{0} (d\sigma/d\cos\theta)\, d\cos\theta}{\int_{-1}^{+1} (d\sigma/d\cos\theta)\, d\cos\theta}. \tag{2}$$

The Standard Model prediction of the asymmetry on the Z^0 peak at lowest order, neglecting the photon-exchange contribution, has the form

$$A_{FB}^0 \approx \frac{3}{4} \left(\frac{2 g_V^e g_A^e}{(g_V^e)^2 + (g_A^e)^2} \right) \left(\frac{2 g_V^f g_A^f}{(g_V^f)^2 + (g_A^f)^2} \right), \tag{3}$$

where g_V and g_A are the vector and axial-vector couplings of the electron and fermion, f, to the Z^0. The effective weak mixing parameter for charged fermions can be expressed as

$$\sin^2 \theta_W^{eff,f} = \frac{1}{4|q_f|} \left(1 - \frac{g_V^f}{g_A^f} \right), \tag{4}$$

where q_f is the electric charge of the fermion in units of the electron charge. Hence, measuring A_{FB} allows the weak mixing angle to be determined within the Standard Model. The asymmetry for down-like (d, s, b) quarks has a larger sensitivity to the weak mixing angle than that for up-like (u, c) quarks and charged leptons [1]. The asymmetry depends on the centre-of-mass energy because of the changing sizes of the Z^0 γ interference. This dependence is well defined within the Standard Model [1].

Three techniques have previously been used to measure the b quark asymmetry, A_{FB}^b, at LEP: jet charge [2, 3], high p_T leptons [4], and D mesons [5]. Here we present measurements of A_{FB}^b using data collected by OPAL in 1991–1995 at centre-of-mass energies on and approximately 2 GeV above and below the Z^0 peak. The measurements use a jet charge technique [3] together with a novel vertex charge method. The additional information contained in the vertex charge and the inclusion of data collected in 1995 have led to an improvement in statistical precision, especially for the off-peak points.

The next section describes the event selection, the Monte Carlo simulation, and the tagging of $Z^0 \to b\bar{b}$ events using reconstructed secondary vertices significantly displaced from the interaction point. Section 3 describes the vertex charge method, where impact parameter information was used to estimate the charge of the hadron whose decay produces the secondary vertex. A sample of events was selected where the vertex charge was a reliable estimator of the quark charge. A maximum likelihood fitting procedure was used to find the observed asymmetry in this sample. The asymmetry in the events which were lifetime tagged but not used in the vertex charge analysis was found using the jet charge method described in section 4. This uses the mean difference between the jet charge in the forward and backward hemispheres.

To extract $A_{\rm FB}^{\rm b}$ from the observed asymmetries the flavour composition of each sample was required. This was obtained with an unfolding technique described in section 5. The performance of the jet and vertex charge are determined from data. This is described in section 6.

The measured values of $A_{\rm FB}^{\rm b}$ are shown in section 7. The values of the asymmetry obtained with the two methods were combined. The estimation of the systematic errors is discussed in section 8. Finally the results are interpreted within the Standard Model in section 9.

2 Event selection

The analysis was performed on events collected by the OPAL detector [6] in the years 1991–1995. Of particular importance for this analysis are the vertex detectors. To account for small modifications made to these detectors the analysis has been done separately for the data collected in 1991–1992, 1993, and 1994–1995 and combined. Multihadronic decays of the $\rm Z^0$ were selected using the criteria described in [7]. They were required to have at least seven charged tracks which passed track quality cuts. The thrust axis, which has been shown to be a good estimator of the direction of the primary quark-antiquark pair, was calculated for each event using tracks and the energy clusters in the electromagnetic calorimeter not associated to tracks. Each event was split into two hemispheres by a plane which was perpendicular to the thrust axis and contained the interaction point. The hemispheres that contained the positive z axis[1] were labelled 'forward thrust hemispheres', the others 'backward thrust hemispheres'. Events were only accepted if the polar angle of the thrust axis, $\theta_{\rm T}$, satisfied $|\cos\theta_{\rm T}| < 0.8$. This ensured that the events were mostly restricted to the silicon micro-vertex detector acceptance.

For the purpose of b-tagging, tracks and unassociated electromagnetic clusters were combined into jets using the JADE algorithm [8], with the E0 recombination scheme [9], and an invariant mass cut-off of $x_{\rm min} = 49({\rm GeV}/c^2)^2$. The Monte Carlo simulation showed that these jet directions were good estimators of the b hadron direction.

Simulated events were generated using the JETSET 7.3 and JETSET 7.4 models [10] and were passed through a program which simulates the response of the OPAL detector [11]. The parameters of the JETSET generators were tuned to optimise the description of OPAL data [12, 13]. The differences between the Monte Carlo models were used in the systematic error estimation. Light quark hadronisation was modelled with the Lund symmetric fragmentation function [10], while the hadronisation of b and c quarks was described by the fragmentation function of Peterson *et al.* [14]. A smaller sample of events generated with the HERWIG 5.6 [15] model was used for checks of possible systematic effects.

A lifetime tag [16] was used to tag $\rm Z^0$ to $\rm b\overline{b}$ decay events. Events were tagged if they contained a secondary vertex which was well separated from the primary vertex. The primary vertex was reconstructed from all tracks in the event, together with a constraint to the average beamspot position. A secondary vertex was searched for by combining all tracks in a jet into a common vertex in the plane transverse to the beam direction. Tracks were only considered if they passed tighter quality requirements designed to reject poorly measured tracks and those from long-lived particles like $\rm K_s^0$ or Λ. The χ^2 of this vertex was calculated, and tracks were removed in an iterative procedure, until no track contributed more than four to the χ^2, or less

[1] The OPAL coordinate system is defined with positive z along the electron beam direction with θ and ϕ being the polar and azimuthal angles, respectively. The origin is in the centre of the detector, which is the nominal interaction point.

than four tracks remained in the vertex. The last requirement reduced significantly the charm background.

The 'vertex decay length', L, was defined as the distance between the secondary vertex and the primary vertex in the r-ϕ plane, and was constrained to the direction of the total momentum vector of the jet containing the secondary vertex projected into the $r-\phi$ plane. The decay length was signed positive if the secondary vertex was displaced from the primary vertex in the same direction as the jet momentum, otherwise it was signed negative. Vertices were required to have a reconstructed decay length $|L| < 2\,\mathrm{cm}$. The error on the decay length, σ_L, comes mainly from the uncertainty in the secondary vertex position, though there is also a small contribution from the primary vertex. Tagged hemispheres had to have at least one vertex with a decay length significance, L/σ_L, greater than 4. This value was found to minimise the total error on the measured on-peak asymmetry. The lifetime tagged sample contained approximately 83% bottom, 11% charm and 6% light quark events. Figure 1 shows the L/σ_L distribution for the data and Monte Carlo. As the analysis was performed separately for the data collected in different years, Figure 1 and subsequent figures show the 1994–1995 data sample and Monte Carlo unless explicitly stated. In all cases the differences between the years were small.

As the asymmetry depends strongly on the centre-of-mass energy, it was measured separately below, on, and above the Z^0 peak. The energy ranges which defined the peak$-$2, peak, and peak+2 samples are shown in table 1, along with the mean centre-of-mass energies, $\langle\sqrt{s}\rangle$. The number of events passing the acceptance cut, N_{had}, the number of tagged hemispheres, N_{t}, and the number of events with both hemispheres tagged, N_{tt}, are also shown.

	$\sqrt{s}$ range (GeV)	$\langle\sqrt{s}\rangle$ (GeV)	N_{had}	N_{t}	N_{tt}
peak$-$2	88.40–90.40	89.44	140133	20631	2571
peak	91.05–91.40	91.21	2365545	350383	42974
peak+2	91.80–94.00	92.91	211178	31471	3855

Table 1: The mean centre-of-mass energies and number of events in the full data sample.

3 The vertex charge analysis

The 'vertex charge', q_{vtx}, is a weighted sum of the charges of tracks in a jet which contains a tagged secondary vertex:

$$q_{\mathrm{vtx}} = \sum_{\mathrm{tracks}\ i} \omega_i q_i, \tag{5}$$

where q_i is the charge of track i, and ω_i is related to the probability that a track came from the secondary vertex relative to the probability that it came from the primary vertex, and i runs over all tracks in the jet. The vertex charge has been shown to be a good estimator of the charge of the long-lived hadron which decays to produce the reconstructed secondary vertex [17]. The weight ω_i is calculated using impact parameter, momentum, and multiplicity information:

$$\omega_i = \frac{R_{\mathrm{sec}}(b_i/\zeta_i)}{R_{\mathrm{sec}}(b_i/\zeta_i) + R_{\mathrm{prim}}(d_i/\sigma_i)}, \tag{6}$$

where $R_{\rm prim,sec}$ are functions modelling the impact parameter significance for a track i relative to a fitted vertex (primary or secondary), b and ζ are the impact parameter and its uncertainty in the plane transverse to the beam axis, with respect to the secondary vertex, and d and σ are the corresponding quantities for the primary vertex. Two different functions $R_{\rm prim}$ and $R_{\rm sec}$ are needed to take into account different mean multiplicities and track momentum spectra. Figure 2a shows the vertex charge distribution for all lifetime tagged jets.

An estimate of the accuracy of each $q_{\rm vtx}$ can be made from the variance:

$$\sigma_q^2 \;=\; \sum_{\text{tracks } i} \omega_i(1-\omega_i)q_i^2. \tag{7}$$

Any ambiguity in assigning the tracks to either the primary or secondary vertex will lead to a non-zero variance.

The vertex charge was calculated for the lifetime tagged jets. To measure the asymmetry the charge of the quark in the forward or backward hemisphere was required. As the charge of neutral mesons gave no information about the heavy quark charge these were removed by requiring $|q_{\rm vtx}| > 1.4\sigma_q + 0.2$. This cut also removed poorly determined vertex charges. As the charm background in the lifetime tagged sample was principally composed of charged D mesons because of their long lifetimes, this cut removed few charm events. A significant fraction of the tagged events were $\rm B^0$s, which were removed by the cut, increasing the charm fraction in the sample. Almost all of this charm background was removed by making a strict requirement on the output of an artificial neural network which was trained to discriminate between b and non-b vertices using the vertex invariant mass and multiplicity, and the track impact parameters [17].

The hemispheres which contain a jet passing the $|q_{\rm vtx}|$ and neural network cuts are said to be '$q_{\rm vtx}$-tagged'. In the total data set there were 12889 $q_{\rm vtx}$-tagged hemispheres, and 65 events with a $q_{\rm vtx}$ tag in both hemispheres; 2920 events had a $q_{\rm vtx}$ tag in one hemisphere and a lifetime tag in the other.

Figure 2b shows the data and Monte Carlo $q_{\rm vtx}$ distribution in the $q_{\rm vtx}$-tagged hemispheres. Figure 2c shows the same Monte Carlo distribution split into the contributions from hemispheres containing positively and negatively charged quarks.

An unbinned maximum likelihood fit was used to obtain the observed asymmetry, $A_{\rm FB}^{\rm obs}$, in the small $q_{\rm vtx}$-tagged sample. If there was a well defined vertex charge in both hemispheres the orientation of the quark and antiquark was very well known, so these events were analysed separately. The $q_{\rm vtx}$-tagged sample was therefore split into two subsets: events with one $q_{\rm vtx}$ tag, labelled '1q', and events with one tag in each hemisphere, labelled '2q'. In 18 of the 65 double $q_{\rm vtx}$-tagged events the two vertex charges had the same sign. These give no information on the asymmetry, so the vertex charge with the smallest $|q_{\rm vtx}|/\sigma_q$ was ignored and the event was reclassified to be in the subset '1q'. The sign of $q_{\rm vtx}$ was used as the estimator of the sign of the charge of the primary quark in that hemisphere which in turn gave the orientation of the $\rm q\bar{q}$ pair. The log likelihood which was maximised to find $A_{\rm FB}^{\rm obs}$ is

$$\ln\mathcal{L} \;=\; \sum_{\text{events } j} \ln(1 + x_j^2 + \frac{8}{3}\beta_j x_j \frac{q_{{\rm vtx},j}}{|q_{{\rm vtx},j}|} A_{\rm FB}^{\rm obs}), \tag{8}$$

where x_j is $|\cos\theta_{\rm T}|$ and β_j is $-1(+1)$ if the $q_{\rm vtx}$ tagged vertex is in the forward (backward) hemisphere.

The fitted observed asymmetry $A_{\rm FB}^{\rm obs}$ had contributions from the charm and light quark background and was degraded because the sign of the reconstructed vertex charge was not a

perfect estimator of the charge of the primary quark. The observed asymmetry can be related to the b asymmetry if the performance of the vertex charge and the fraction of non-b events in the sample are known. This performance is defined by the reliability P_i^q, the probability that the sign of the vertex charge is equal to the sign of the primary quark in the event.

In events with only one vertex charge the asymmetry is given by:

$$A_{\rm FB}^{\rm obs} = \sum_{\text{flavours } f} s_f F_f^{(1q)} (2P_f^q - 1) A_{\rm FB}^f; \tag{9}$$

similarly for events with a vertex charge in each hemisphere it is:

$$A_{\rm FB}^{\rm obs} = \sum_{\text{flavours } f} s_f F_f^{(2q)} \frac{(P_f^q)^2\alpha_1 - (1-P_f^q)^2\alpha_2}{(P_f^q)^2\alpha_1 + (1-P_f^q)^2\alpha_2} A_{\rm FB}^f, \tag{10}$$

where $F_f^{(1q)}$ and $F_f^{(2q)}$ are the fractions of each flavour in the single $q_{\rm vtx}$- and double $q_{\rm vtx}$-tagged events respectively. The quantity s_i is $+1(-1)$ for down-like (up-like) quark flavours. The determination of the fractions $F_f^{(1q)}$ and $F_f^{(2q)}$ and the reliability of the vertex charge in b events, $P_{\rm b}^q$, are described in sections 5 and 6 respectively. The reliabilities in the charm and light quark events were taken from Monte Carlo simulations. Any correlations between the $q_{\rm vtx}$ values in opposite hemispheres, other than that due to quark-antiquark production, are accounted for by the α_1 and α_2 terms which were close to one and taken from the Monte Carlo. Standard Model values of the non-b asymmetries were used and the equations were inverted to give $A_{\rm FB}^{\rm b}$. The two extracted values of $A_{\rm FB}^{\rm b}$ were compatible and were combined. The results from this analysis are discussed in section 7.

4 The jet charge analysis

The jet charge technique was used to measure the asymmetry in events which were not $q_{\rm vtx}$ tagged. As the events with large $|\cos\theta_{\rm T}|$ show a greater asymmetry than those with small $|\cos\theta_{\rm T}|$, the precision was improved by performing the jet charge analysis in four bins of $|\cos\theta_{\rm T}|$ (0.0–0.2, 0.2–0.4, 0.4–0.6 and 0.6–0.8). The values measured in each bin were combined.

The jet charge was calculated by summing over all tracks in a thrust hemisphere:

$$Q_{\rm jet} = \frac{\sum |p_{||,i}|^\kappa q_i}{\sum |p_{||,i}|^\kappa}, \tag{11}$$

where $p_{||,i}$ is the component of momentum parallel to the thrust axis, and q_i is the charge of track i in the hemisphere. The exponent κ was set to 0.5; this value was found to minimise the on-peak $A_{\rm FB}^{\rm b}$ total error. The jet charges in the forward and backward thrust hemispheres are labelled Q_F and Q_B respectively. The jet charge for the hemisphere containing the negative primary quark is labelled Q_- and that for the positive primary quark Q_+. The charge separation is defined as $\delta = \langle Q_- - Q_+ \rangle$ and the charge flow as $\langle Q_F - Q_B \rangle$. For a sample with no charm or light quark background and with no acceptance effects it can be shown that

$$\langle Q_F - Q_B \rangle = \delta \cdot A_{\rm FB}^{\rm b}. \tag{12}$$

For a sample containing a mixture of quark species and a varying tagging efficiency as a function of $|\cos\theta_{\rm T}|$ for each flavour, this becomes

$$\langle Q_F - Q_B \rangle = \sum_{\text{flavours } f} s_f F_f^{(1t)} C^f \delta_f A_{\rm FB}^f, \tag{13}$$

where s_f is $+1(-1)$ for down-like (up-like) quarks, and $F_f^{(\mathrm{lt})}$ is the fraction of quark species f in the lifetime-tagged sample—determined using the unfolding technique described in section 5. The quantity δ_f is the charge separation for flavour f events. The b quark charge separation, δ_b, was measured from the data using the technique described below, while the charm and light quark charge separations were taken from the Monte Carlo. The C^f factors account for the effects of the variation of tagging efficiency with $|\cos\theta_\mathrm{T}|$ and are given by

$$C^f = \frac{8}{3}\frac{\int \bar{\eta}_f(y) y dy}{\int \bar{\eta}_f(y)(1+y^2)dy}, \tag{14}$$

where $y = |\cos\theta_\mathrm{T}|$ and $\bar{\eta}_f(y)$ is the efficiency of lifetime tagging a flavour f event. The event tagging efficiency for b and c events was found from data in many bins of $|\cos\theta_\mathrm{T}|$, using the unfolding method of section 5, and then parameterised. The C factors for the u, d, and s quarks were assumed all to have the same value which was taken from the Monte Carlo. The C factors for the four $|\cos\theta_\mathrm{T}|$ bins are shown in table 2. As the analysis was performed separately for the data collected in different years, table 2 and subsequent tables apply to the 1994–1995 data and Monte Carlo only, unless explicitly stated otherwise. In all cases the values for the other years were similar.

	$\lvert\cos\theta_\mathrm{T}\rvert$ range			
flavour	0.0–0.2	0.2–0.4	0.4–0.6	0.6–0.8
b	0.2604 ± 0.0009	0.7290 ± 0.0007	1.0619 ± 0.0004	1.2463 ± 0.0007
c	0.259 ± 0.002	0.727 ± 0.001	1.0599 ± 0.0004	1.2472 ± 0.0005
d, u, s	0.261 ± 0.001	0.730 ± 0.001	1.0623 ± 0.0006	1.249 ± 0.001

Table 2: The C factors for each $|\cos\theta_\mathrm{T}|$ bin. The b and c quark values were measured in the data; the errors are statistical only. The light quark values were taken from the Monte Carlo; the errors are due to the finite Monte Carlo statistics available.

For a given event flavour, if there is no correlation between the jet charges in opposite hemispheres and the jet charge is unbiased (i.e. the mean jet charge of all hemispheres is zero) the mean charge separation in a sample can be found using the relation

$$\left(\frac{\delta}{2}\right)^2 = -\langle Q_F \cdot Q_B \rangle, \tag{15}$$

where $\langle Q_F \cdot Q_B \rangle$ is measured from the data. However, there was a charge bias in the detector, of approximate size 0.05, as more positively charged tracks were observed than negative ones. There was also a charge correlation due to effects such as charge conservation and hard gluon radiation. The more general expression, derived in Ref. [3], includes such possible effects:

$$\left(\frac{\delta}{2}\right)^2 = \frac{-\langle Q_F \cdot Q_B \rangle + \rho[Q_-, Q_+]\sigma^2(Q) + \mu^2(Q)}{1 + \rho[Q_-, Q_+]}, \tag{16}$$

where $\mu(Q)$ and $\sigma^2(Q)$ are the mean and variance of the jet charge for all hemispheres and were measured from the data. The $\rho[Q_-, Q_+]$ term is the charge correlation between Q_- and Q_+ and was taken from the Monte Carlo. This expression gives the mean charge separation

in a particular sample; as the lifetime-tagged sample was used the charge separation must be corrected for the charm and light quark background. The measured charge separation is

$$\delta^{\text{tagged}} = \sum_{\text{flavours } f} F_f^{(\text{lt})} \delta_f. \tag{17}$$

The equation was inverted using the Monte Carlo predictions for the charm and light quark charge separations to extract δ_{b}. As the charm and light quark fractions in the lifetime-tagged sample were small, no large systematic effect was introduced by using the Monte Carlo predictions. The mean jet charge quantities are shown in table 3.

$\lvert\cos\theta_{\text{T}}\rvert$ range	$\langle Q_F - Q_B \rangle$	δ^{tagged}	δ_{b}
0.0–0.2	-0.002 ± 0.001	-0.132 ± 0.002	-0.130 ± 0.003
0.2–0.4	-0.007 ± 0.001	-0.136 ± 0.002	-0.134 ± 0.003
0.4–0.6	-0.012 ± 0.001	-0.138 ± 0.002	-0.138 ± 0.003
0.6–0.8	-0.014 ± 0.001	-0.137 ± 0.002	-0.135 ± 0.003

Table 3: Measured jet charge properties for each $\lvert\cos\theta_{\text{T}}\rvert$ bin for all the data. The errors are statistical.

5 Measuring the composition of the samples

To extract the true asymmetry, A_{FB}^{b}, from the observed vertex charge asymmetries, using equations 9 and 10, and from the jet charge measurement, using equation 13, the flavour compositions of the three samples were required.

These flavour compositions depend on the flavour mix of the original sample of events, $R_f = \Gamma(\text{Z}^0 \to f\bar{f})/\Gamma(\text{Z}^0 \to \text{hadrons})$, and the efficiencies with which events of each flavour, f, were tagged by each of the three techniques: $\bar{\eta}_f$ for the jet charge sample; $\bar{\xi_f}^{(1\text{q})}$, $\bar{\xi_f}^{(2\text{q})}$ for the vertex charge sample:

$$F_f^{(\text{lt})} = \frac{R_f \bar{\eta}_f}{\sum_k R_k \bar{\eta}_k}, \qquad F_f^{(1\text{q})} = \frac{R_f \bar{\xi_f}^{(1\text{q})}}{\sum_k R_k \bar{\xi_k}^{(1\text{q})}}, \qquad F_f^{(2\text{q})} = \frac{R_f \bar{\xi_f}^{(2\text{q})}}{\sum_k R_k \bar{\xi_k}^{(2\text{q})}}. \tag{18}$$

These event tagging efficiencies were determined separately in each $\lvert\cos\theta_{\text{T}}\rvert$ bin. They are related to the efficiencies for tagging a hemisphere using

$$\bar{\eta}_f = 2\eta_f(1 - \rho_f^{(1)}\eta_i) + \rho_f^{(1)}{\eta_i}^2 - 2\xi_f(1 - \rho_f^{(2)}\xi_f) - \rho_f^{(2)}{\xi_f}^2, \tag{19}$$

$$\bar{\xi_f}^{(1\text{q})} = 2\xi_f(1 - \rho_f^{(2)}\xi_f), \tag{20}$$

$$\bar{\xi_f}^{(2\text{q})} = \rho_f^{(2)}{\xi_f}^2, \tag{21}$$

where $\rho_f^{(1,2)} = 1$ for f = u,d,s and c, ξ_f is the efficiency for tagging a flavour f hemisphere with a q_{vtx} tag, and η_f is the lifetime hemisphere tagging efficiency for the same flavour f. Corrections for double counting are made explicitly in these equations. The ρ terms include the effects of correlations due to physics effects and due to the geometry of the detector.

The charm and light quark contaminations were small so the corresponding correlations ρ were taken to be unity. For the b quark events the geometrical correlation effects were found from the angular dependence of the tagging efficiency [16]; the small correlations coming from physics sources were taken from the Monte Carlo.

The light quark hemisphere efficiencies were taken from the Monte Carlo, and the b and c hemisphere efficiencies were extracted from the data using an extension of the 'double tagging' technique [16]. The number of lifetime-tagged hemispheres, $N_{\rm t}$, and the number of double lifetime-tagged events, $N_{\rm tt}$, were counted. Similarly, the number of $q_{\rm vtx}$-tagged hemispheres, $N_{\rm v}$, the number of double $q_{\rm vtx}$-tagged events, $N_{\rm vv}$, and the number of events which contained a significant vertex charge in one hemisphere and a lifetime tag in the other, $N_{\rm vt}$ were determined. A singular-value decomposition unfolding technique [18] was used to extract the four unknown quantities, $\eta_{\rm b}$, $\eta_{\rm c}$, $\xi_{\rm b}$, and $\xi_{\rm c}$, from the five measured quantities $\{N_{\rm t}, N_{\rm tt}, N_{\rm v}, N_{\rm vv}, N_{\rm vt}\}$, in each $|\cos\theta_{\rm T}|$ bin. If there was little information about a particular efficiency in the data the unfolding procedure constrained the value to the Monte Carlo efficiency, rather than introducing statistical noise into the analysis, reducing the sensitivity to statistical fluctuations in the data. The details of the unfolding procedure are described in the appendix.

The extracted hemisphere efficiencies are shown in figure 3, the flavour compositions for each sample, averaged over all $|\cos\theta_{\rm T}|$ bins, in table 4.

Flavour	jet charge sample	$q_{\rm vtx}$(1q) sample	$q_{\rm vtx}$(2q) sample
b	82.8 ± 0.4	99.2	100.0
c	10.5 ± 0.4	0.6	0.0
s	2.4	0.1	0.0
u	1.9	0.1	0.0
d	2.3	0.1	0.0

Table 4: The fraction (in %) of each flavour in the samples with the data statistical error. Where no error is shown, it is negligible.

6 Measuring the reliability of the vertex charge

The reliability of the vertex charge estimator, $P_{\rm b}^q$, was needed to extract $A_{\rm FB}^{\rm b}$ from the observed asymmetry using equations 9 and 10. In principle it can be determined from events with two vertex tags: if the charge assignment were always correct ($P_{\rm b}^q$=100%) then the two vertex charges would always be of opposite sign; if the charge assignment were random, there would be a 50–50 mixture of opposite-sign and same-sign events.

The number of double $q_{\rm vtx}$-tagged events was too small to determine $P_{\rm b}^q$ precisely using this method. Instead, the larger sample of events with one vertex tag was used in combination with a jet charge tag. The fraction of events where the $q_{\rm vtx}$ tag has the opposite sign to the jet charge in the other hemisphere was found. If the jet charge reliability is known, the vertex charge reliability can be determined.

If the hemisphere with the vertex charge tag is labelled 1, the other one 2, the fraction of observed events with a vertex tag in hemisphere 1, and a jet charge measurement of opposite

sign in hemisphere 2, can be written as

$$f^{\rm obs}(Q_2 \neq q_1) \;=\; \sum_{\text{flavours } f} F_f^{(1q)} f_f(Q_2 \neq q_1), \tag{22}$$

where Q denotes the sign of the jet charge and q the sign of the vertex charge. The value $f_{\rm b}(Q_2 \neq q_1)$ was found by inverting this equation using the Monte Carlo predictions for the charm and light quark fractions $f_f(Q_2 \neq q_1)$, and the fractions $F_f^{(1q)}$ determined above. The fraction $f_{\rm b}(Q_2 \neq q_1)$ for b-quark events is a function of the probabilities $P_{\rm b}^Q$ and $P_{\rm b}^q$, that the sign q_1 of the vertex charge or the sign Q_2 of the jet charge is the same as the sign of the quark in the respective hemisphere. It is given by:

$$f_{\rm b}(Q_2 \neq q_1) \;=\; P_{\rm b}^Q \cdot P_{\rm b}^q \varrho_1' + (1 - P_{\rm b}^Q) \cdot (1 - P_{\rm b}^q) \varrho_2'. \tag{23}$$

The terms ϱ_1' and ϱ_2' account for small correlations between the probabilities in opposite hemispheres. They were taken from Monte Carlo, and are very close to unity. The effect of $\rm B\overline{B}$ mixing is implicitly taken into account in this formalism and absorbed into the probability $P_{\rm b}^q$. Therefore, if $P_{\rm b}^Q$ is known, $P_{\rm b}^q$ can be extracted from the data.

Since the number of events with a good jet charge measurement is much larger than the one with a vertex charge measurement, the probability $P_{\rm b}^Q$ can be determined from the fraction of lifetime-tagged events which had opposite jet charges in the two hemispheres. Its value is found from the observed fraction $f^{\rm obs}(Q_1 \neq Q_2)$ in the lifetime-tagged event sample by inverting:

$$f^{\rm obs}(Q_1 \neq Q_2) \;=\; \sum_{\text{flavours } i} F_f^{(1t)} f_i(Q_1 \neq Q_2). \tag{24}$$

using $F_f^{(1t)}$ determined above and the Monte Carlo predictions for the charm and light quark fractions. Following equation 23 the b quark fraction, $f_{\rm b}(Q_1 \neq Q_2)$, can be written as:

$$f_{\rm b}(Q_1 \neq Q_2) \;=\; (P_{\rm b}^Q)^2 \varrho_1 + (1 - P_{\rm b}^Q)^2 \varrho_2. \tag{25}$$

The correlation terms ϱ_1 and ϱ_2 were again extracted from Monte Carlo. This value of $P_{\rm b}^Q$ was used to extract $P_{\rm b}^q$ using equation 23.

Equation 25 is only true if both the jet charge and the vertex charge tagged hemispheres are unbiased. However the presence of a lifetime tag in a hemisphere will bias the jet charge in that hemisphere and in turn bias the measured jet charge probability $P_{\rm b}^Q$. This bias results from both the multiplicity cut and decay length significance cut, which requires that the B hadron has a large boost. To extract $P_{\rm b}^q$ using equation 23 the value of $P_{\rm b}^Q$ in untagged hemispheres was required. The size of this bias was found from the Monte Carlo, and equation 25 was modified to include it. The quantities used in the extraction of $P_{\rm b}^q$ are shown in table 5 for both Monte Carlo and data.

7 The b quark asymmetry

As the off-peak data samples were relatively small it was assumed that all the quantities, except $\langle Q_F - Q_B \rangle$ and the log likelihood sum, were the same for all energy points. A possible dependence of $\delta_{\rm b}$ on $\sqrt{s}$ was investigated by examining $\langle Q_F \cdot Q_B \rangle$ in each energy window. No

	Monte Carlo	Data
$f^{\rm obs}(Q_1 \neq Q_2)$	0.5509 ± 0.0006	0.551 ± 0.001
$P_{\rm b}^{Q}$	0.6441 ± 0.0003	0.646 ± 0.004
$f^{\rm obs}(Q_1 \neq q_2)$	0.598 ± 0.003	0.590 ± 0.006
$P_{\rm b}^{q}$	0.828 ± 0.002	0.79 ± 0.03

Table 5: Jet charge and vertex charge probabilities and fractions of events tagged with two oppositely signed jet charge measurements or vertex charge measurements in the two hemispheres of the event. Shown are results for both Monte Carlo and data. The errors are statistical only. The values are consistent.

trend was observed except the one coming from the small correlation between $\langle Q_F \cdot Q_B \rangle$ and $\langle Q_F - Q_B \rangle$ (which depends on $\sqrt{s}$ through $A_{\rm FB}^{\rm b}$).

The central $A_{\rm FB}^{\rm b}$ values were derived using the Standard Model expectations for the other flavours shown in table 6. These were calculated with the ZFITTER 5.0 [19] package, for a top quark mass of 175 GeV. The asymmetries measured with each method in each of the periods 1991–1992, 1993, and 1994–1995 were compatible. Table 7 shows the values for each method averaged over the three periods 1991–1992, 1993, and 1994–1995, in bins of $\cos\theta_{\rm T}$. The overall weighted average for each energy point is also shown. The results of the measurement are illustrated in figure 4, for all three energies. Shown is the measured charge flow, $\langle Q_F - Q_B \rangle$, plotted as a function of $\cos\theta_{\rm T}$. The same quantity, calculated from the measured asymmetries and taking into account the light flavour and charm background as given by equation 13, is shown as the line histogram in the same figure.

The measured asymmetry used the reconstructed thrust axis as an approximation for the event axis. This is not exactly the same as the asymmetry calculated relative to the direction of the primary quark-antiquark pair, or relative to the thrust axis calculated using all particles before detector effects (hadron level thrust axis). The correction factors were taken from the Monte Carlo simulation. The hadron level thrust axis asymmetries were found to be smaller than the experimental thrust axis asymmetries by a multiplicative factor of 0.989. The quark axis asymmetries were larger than the experimental thrust axis asymmetries by a factor 1.010. In general these factors are independent of the centre-of-mass energy. Calculated for this analysis the results are shifted by -0.00045, -0.00109 and -0.00160 to arrive at the hadron-level thrust asymmetries, and $+0.00043$, $+0.00102$ and $+0.00149$ to get the quark axis asymmetries. Since Monte Carlo is used for the calculation of these corrections they include both QCD and QED effects. Note however that the total correction is significantly smaller than the ones obtained for other analyses [22]. This is mostly because the calibration of the jet and vertex charge measurements in data implicitly includes a large part of the QCD corrections and absorbs them into the jet and vertex charge reliabilities.

8 The systematic errors

8.1 Fragmentation and decay modelling

To obtain an estimate of the systematic errors connected with event shape variables, the mean charge multiplicity in c and b events, single particle momentum spectra and single particle

Flavour	R_f	$A_{\rm FB}^f(\sqrt{s} = 89.44\,{\rm GeV})$	$A_{\rm FB}^f(\sqrt{s} = 91.21\,{\rm GeV})$	$A_{\rm FB}^f(\sqrt{s} = 92.91\,{\rm GeV})$
$b\overline{b}$	0.215	–	–	–
$c\overline{c}$	0.173	−0.0347	0.0595	0.120
$s\overline{s}$	0.220	0.0565	0.0936	0.117
$u\overline{u}$	0.173	−0.0345	0.0594	0.120
$d\overline{d}$	0.220	0.0565	0.0936	0.117

Table 6: The values of the Standard Model parameters as given by ZFITTER and as used in the calculation of the b-forward backward asymmetry.

inclusive production rates, their values were varied in the Monte Carlo within the bounds given in [12, 13]. Previous studies [3] have shown that the asymmetry analysis depends in particular on the Peterson parameter for heavy flavour fragmentation, the "popcorn parameter" connected to baryon production, and the probability that a light meson is produced with spin 1 or spin 0. Each of these parameters has been changed by approximately one standard deviation, as described in [13]. Additionally the predictions of the OPAL tuned HERWIG 5.6 Monte Carlo sample were used.

The most significant inputs for the jet charge analysis were the jet charge correlation $\rho[Q_-, Q_+]$, and the charm charge separation $\delta_{\rm c}$. Inputs for the $q_{\rm vtx}$ analysis were the probabilities of a correct sign jet charge in charm events $P_{\rm c}^Q$, the correlations in equation 25 and 23, and the bias in $P_{\rm b}^Q$ due to the lifetime tagging. The level of uncertainty in these parameters was estimated from the largest difference found when they were recalculated for the different input parameters, or in the different Monte Carlos. Table 8 shows the variation of the measured $A_{\rm FB}^{\rm b}$ when these Monte Carlo parameters were varied up and down by half their uncertainty. The systematic error from the uncertainty on the bias on $P_{\rm b}^Q$ was conservatively estimated by removing and doubling it.

As a cross check, systematic errors due to fragmentation models were estimated using many Monte Carlo samples with a simplified detector geometry, with different fragmentation parameters. This gave a slightly smaller error than the one quoted above, and the above estimation was used.

The effect of uncertainties of b- and c-hadron decay multiplicities in the Monte Carlo was found by reweighting Monte Carlo events. They were first weighted so that the multiplicity distributions were Poisson with the mean of the unweighted sample. They were then reweighted to a Poisson with a different mean. The change in asymmetry caused by the reweighting was assigned to be the systematic error. The mean b-hadron decay multiplicity was varied by the OPAL measured uncertainty of ± 0.51 [20]. The mean charm decay multiplicity was varied by ± 0.06 [21].

The total error for fragmentation and decay modelling effects was found to be ± 0.0011, ± 0.0031, ± 0.0052 for the peak-2, peak, and peak$+2$ asymmetries, respectively.

8.2 Tagging and detector simulation

The acceptance factors, C^i, were obtained using the JETSET Monte Carlo for the light quark events. The change in $A_{\rm FB}^{\rm b}$ when the predictions of HERWIG 5.6 were used was taken as an estimate of the systematic uncertainties from the modelling of the acceptances.

Method		$A_{\rm FB}^{\rm b}$		
peak$-$2				
vertex charge		0.104	$\pm$	0.069
jet charge	$0.0 \leq \lvert\cos\theta_{\rm T}\rvert < 0.2$	0.34	$\pm$	0.17
	$0.2 \leq \lvert\cos\theta_{\rm T}\rvert < 0.4$	0.103	$\pm$	0.059
	$0.4 \leq \lvert\cos\theta_{\rm T}\rvert < 0.6$	0.020	$\pm$	0.038
	$0.6 \leq \lvert\cos\theta_{\rm T}\rvert < 0.8$	0.016	$\pm$	0.032
Combined		0.041	$\pm$	0.021
peak				
vertex charge		0.087	$\pm$	0.018
jet charge	$0.0 \leq \lvert\cos\theta_{\rm T}\rvert < 0.2$	0.092	$\pm$	0.043
	$0.2 \leq \lvert\cos\theta_{\rm T}\rvert < 0.4$	0.090	$\pm$	0.015
	$0.4 \leq \lvert\cos\theta_{\rm T}\rvert < 0.6$	0.1033	$\pm$	0.0094
	$0.6 \leq \lvert\cos\theta_{\rm T}\rvert < 0.8$	0.1046	$\pm$	0.0079
Combined		0.1005	$\pm$	0.0053
peak+2				
vertex charge		0.172	$\pm$	0.055
jet charge	$0.0 \leq \lvert\cos\theta_{\rm T}\rvert < 0.2$	-0.01	$\pm$	0.14
	$0.2 \leq \lvert\cos\theta_{\rm T}\rvert < 0.4$	0.182	$\pm$	0.048
	$0.4 \leq \lvert\cos\theta_{\rm T}\rvert < 0.6$	0.165	$\pm$	0.030
	$0.6 \leq \lvert\cos\theta_{\rm T}\rvert < 0.8$	0.124	$\pm$	0.026
Combined		0.147	$\pm$	0.017

Table 7: The values of the asymmetry found using the complete 1991-1995 data sample for each energy range. The statistical errors are shown. The values quoted have not been corrected for the effects of the detector resolution on the thrust axis.

The values for the light quark lifetime tagging efficiencies were found from the Monte Carlo. The systematic error associated with these efficiencies was found by scaling the light quark efficiencies by 10%.

The expression for the log likelihood assumes that the angular dependence of the efficiency is the same for all quark species. However, as the charm and light quark fraction in the $q_{\rm vtx}$ sample were small no systematic shift was introduced by this assumption. Additionally the dependence of $P_{\rm b}^{q}$ on $|\cos\theta_{\rm T}|$ was investigated. No significant effect was found.

The correlations in the equations 26–30 arise from detector and physics effects. As the b efficiencies $\xi_{\rm b}$ and $\eta_{\rm b}$ were much larger than the charm and light quark efficiencies, only the correlations for b quark events were important. The value of $\rho_{\rm b}^{(2)}$ was assumed to be the same as $\rho_{\rm b}^{(1)}$ for the central value. The systematic error was found from the shift in the asymmetry when they were varied between 1 and $1 + 2(\rho - 1)$.

The Monte Carlo tracking resolution in the plane transverse to the beam direction was adjusted to reproduce the data in the region of negative decay length significance. To estimate the systematics from this, the resolution was varied by 10%. The uncertainty due to the Monte Carlo z-direction resolution was found by degrading the z track parameter resolution by a factor two.

quantity	peak-2	peak	peak$+2$
$\rho[Q_-, Q_+]$	∓ 0.00064	∓ 0.00132	∓ 0.00195
$\delta_{\rm c}$	∓ 0.00019	∓ 0.00198	∓ 0.00336
$P_{\rm c}^Q$	∓ 0.00005	∓ 0.00021	∓ 0.00025
ϱ_1	∓ 0.00002	∓ 0.00015	∓ 0.00018
ϱ_2	∓ 0.00012	∓ 0.00032	∓ 0.00039
ϱ_1'	± 0.00022	± 0.00112	± 0.00129
Bias in $P_{\rm b}^Q$	± 0.00001	± 0.00008	± 0.00009
c decay multiplicity	± 0.00004	± 0.00022	± 0.00038
b decay multiplicity	± 0.00005	± 0.00033	± 0.00041
Fragmentation and decay	± 0.0011	± 0.0031	± 0.0052
C factor modelling	± 0.00002	± 0.00001	± 0.00004
u, d, s efficiency	± 0.00140	± 0.00149	± 0.00247
hemisphere correlation	± 0.00002	± 0.00098	± 0.00155
r-ϕ detector resolution	± 0.00037	± 0.00149	± 0.00238
z detector resolution	± 0.00131	± 0.00133	± 0.00180
thrust direction resolution	± 0.00045	± 0.00109	± 0.00160
material asymmetry	± 0.00062	± 0.00062	± 0.00062
Detector modelling	± 0.0021	± 0.0030	± 0.0045
Monte Carlo statistics	± 0.0006	± 0.0008	± 0.0012
Total systematics	± 0.0024	± 0.0044	± 0.0070

Table 8: The systematic errors for the combined asymmetry found using the 1991–1995 data sample. More details of the individual errors can be found in the text.

The asymmetry was corrected using the Monte Carlo to account for the differences between the experimental thrust axis, the hadron-level thrust axis, and the axis defined by the quark direction. The sizes of the corrections were taken as an additional systematic error.

An important assumption in the measurement of the asymmetry is that the detector is symmetric for the detection of opposite charged particles, as a function of $|\cos\theta_{\rm T}|$. If the detector is asymmetric it may bias the asymmetry measured with the jet charge. Material causes secondary interactions, increasing the number of positive tracks, so making the jet charge more positive. If this effect is different in the forward and backward hemispheres, it will bias $\langle Q_F - Q_B \rangle$ and hence the measured asymmetry. The bias in the asymmetry can be measured from the asymmetry in the number of γ conversions. The conversion asymmetry has been determined [3] to be consistent with zero within a 0.7% statistical error. If the conversion asymmetry is assumed to be the size of its statistical error then $\delta A = \pm 0.00067$ for the jet charge measurements.

A $q_{\rm vtx}$-tagging efficiency which is asymmetric in $\cos\theta_{\rm T}$ and which is different for positive and negative b hadrons will bias the measurement in the $q_{\rm vtx}$-tagged sample. The bias was estimated from the data to be -0.00013 and was assigned to be the systematic error associated with the material asymmetry.

The total systematic errors assigned to resolution and simulation effects were ± 0.0021, ± 0.0030 and ± 0.0045 for the peak-2, peak and peak+2 points respectively.

8.3 The total systematic error

The systematic errors are shown in table 8. The total systematic error has been calculated as the sum in quadrature of the errors due to fragmentation and decay modelling, detector and simulation effects, and due to Monte Carlo statistics. They were ± 0.0024, ± 0.0044, ± 0.0070 for the peak-2, peak, and peak$+2$ asymmetries respectively.

8.4 Dependence on Standard Model parameters

The measurement of the b quark asymmetry presented in this paper assumes the Standard Model values of the fraction of each quark flavour in the hadronic event sample, R_f, and the forward-backward asymmetries for flavours other than b. In particular for combining this analysis with others at LEP it is important that the dependence of the b-quark asymmetry on the different Standard Model parameters is known. The dependencies have been determined by repeating the analysis after changing the input parameters. The resulting gradients are shown in table 9.

Parameter x	$g(x)$ (peak-2)	$g(x)$ (peak)	$g(x)$ (peak$+2$)
R_{b}	-0.034	-0.355	-0.599
R_{c}	$+0.004$	$+0.027$	$+0.040$
R_{s}	$\lvert g\rvert < 0.001$	$\lvert g\rvert < 0.001$	$\lvert g\rvert < 0.001$
R_{u}	$+0.006$	$+0.034$	$+0.053$
$A_{\mathrm{FB}}^{\mathrm{c}}$	$+0.113$	$+0.111$	$+0.110$
$A_{\mathrm{FB}}^{\mathrm{s}}$	-0.032	-0.032	-0.032
$A_{\mathrm{FB}}^{\mathrm{u}}$	$+0.035$	$+0.035$	$+0.035$
$A_{\mathrm{FB}}^{\mathrm{d}}$	-0.026	-0.026	-0.026

Table 9: The gradients $g(x) = dA/dx$ of $A_{\mathrm{FB}}^{\mathrm{b}}$ found in the 1991–1995 data sample with respect to the assumed Standard Model parameters, x. For this table the partial width R_{d} has been constrained by the condition $R_{\mathrm{d}} = 1 - R_{\mathrm{b}} - R_{\mathrm{c}} - R_{\mathrm{s}} - R_{\mathrm{u}}$.

9 Results

The b forward-backward asymmetry has been measured using jet charge and vertex charge estimators. The asymmetries corrected to the hadron-level thrust axis are

$$\begin{aligned} A_{\mathrm{FB}}^{\mathrm{b}} &= 0.041 \pm 0.021 \pm 0.002 && \sqrt{s} = 89.44 \text{ GeV} \\ A_{\mathrm{FB}}^{\mathrm{b}} &= 0.0994 \pm 0.0052 \pm 0.0044 && \sqrt{s} = 91.21 \text{ GeV} \\ A_{\mathrm{FB}}^{\mathrm{b}} &= 0.145 \pm 0.017 \pm 0.007 && \sqrt{s} = 92.91 \text{ GeV} \end{aligned}$$

where in each case the first error is statistical, the second systematic.

These measurements supersede the previous measurements of the b asymmetry using jet charge made by OPAL [3]. They are more precise due both to more data and the inclusion of the vertex charge method. The results are compatible with those presented in [3] and with other measurements made at LEP [2, 4, 5]. The measured asymmetries, along with the Standard Model predictions, are shown in figure 5.

From the bottom forward–backward asymmetry the weak mixing angle can be extracted. Its value was found using a χ^2 fit between the measured results at the three energy points and the asymmetries calculated using ZFITTER 5.0 [19]. Since ZFITTER does a calculation on the quark level, and does not take detector or fragmentation effects into account, the measured asymmetries have been corrected to the quark level, as described in section 7. The values at the primary quark level are

$$\begin{array}{lll} A_{\rm FB}^{\rm b} = 0.041 \pm 0.021 \pm 0.002 & \sqrt{s} = 89.44 \text{ GeV} \\ A_{\rm FB}^{\rm b} = 0.1015 \pm 0.0054 \pm 0.0044 & \sqrt{s} = 91.21 \text{ GeV} \\ A_{\rm FB}^{\rm b} = 0.148 \pm 0.017 \pm 0.007 & \sqrt{s} = 92.91 \text{ GeV} \end{array}$$

where in each case the first error is statistical, the second systematic. The small correlations between the three measurements were taken into account in the fit. The fit has a χ^2 of 1.73 for 2 degrees of freedom. The extracted weak mixing angle is

$$\sin^2\theta_{\rm W}^{\rm eff,e} = 0.2308 \pm 0.0013.$$

A Higgs boson mass of 300 GeV has been used for this result. The error includes a contribution of $\pm^{0.00003}_{0.00001}$ for a variation of the higgs mass between 60 and 1000 GeV.

Appendix: The unfolding procedure

The quantities $\{N_{\rm t}, N_{\rm tt}, N_{\rm v}, N_{\rm vv}, N_{\rm vt}\}$ were expressed in terms of the quark fractions in the hadronic sample and the hemisphere tagging efficiencies:

$$\begin{aligned} N_{\rm t} &= 2N_{\rm had}(R_{\rm b}\eta_{\rm b} + R_{\rm c}\eta_{\rm c} + R_{\rm s}\eta_{\rm s} + R_{\rm u}\eta_{\rm u} + R_{\rm d}\eta_{\rm d}) && (26)\\ N_{\rm tt} &= N_{\rm had}(R_{\rm b}\eta_{\rm b}^2\rho_{\rm b}^{(1)} + R_{\rm c}\eta_c^2 + R_{\rm s}\eta_{\rm s}^2 + R_{\rm u}\eta_{\rm u}^2 + R_d\eta_{\rm d}^2) && (27)\\ N_{\rm v} &= 2N_{\rm had}(R_{\rm b}\xi_{\rm b} + R_{\rm c}\xi_{\rm c} + R_{\rm s}\xi_{\rm s} + R_{\rm u}\xi_{\rm u} + R_{\rm d}\xi_{\rm d}) && (28)\\ N_{\rm vv} &= N_{\rm had}(R_{\rm b}\xi_{\rm b}^2\rho_{\rm b}^{(2)} + R_{\rm c}\xi_{\rm c}^2 + R_{\rm s}\xi_{\rm s}^2 + R_{\rm u}\xi_{\rm u}^2 + R_{\rm d}\xi_{\rm d}^2) && (29)\\ N_{\rm vt} &= 2N_{\rm had}(R_{\rm b}\eta_{\rm b}\xi_{\rm b}\rho_{\rm b}^{(3)} + R_{\rm c}\eta_{\rm c}\xi_{\rm c} + R_{\rm s}\eta_{\rm s}\xi_{\rm s} + R_{\rm u}\eta_{\rm u}\xi_{\rm u} + R_{\rm d}\xi_{\rm d}\eta_{\rm d}). && (30) \end{aligned}$$

The equations 26 to 30 were transformed so that the measured quantities (the left-hand sides) were independent samples of events:

$$\begin{aligned} n_1' &= N_{\rm t} - N_{\rm tt} - N_{\rm v} + N_{\rm vt} && (31)\\ n_2' &= N_{\rm tt} - N_{\rm vt} && (32)\\ n_3' &= N_{\rm v} - N_{\rm vt} && (33)\\ n_4' &= N_{\rm vt} - N_{\rm vv} && (34)\\ n_5' &= N_{\rm vv}. && (35) \end{aligned}$$

The above equations can be expressed as a linear matrix equation if they are linear in the efficiencies. This is done by rewriting the efficiencies in terms of a trial efficiency which was initially the Monte Carlo value:

$$\begin{aligned} \eta_{\rm b,c}^{\rm data} &= \eta_{\rm b,c}^{\rm trial}(1 + \Delta\eta_{\rm b,c}) && (36)\\ \xi_{\rm b,c}^{\rm data} &= \xi_{\rm b,c}^{\rm trial}(1 + \Delta\xi_{\rm b,c}). && (37) \end{aligned}$$

If $\Delta\eta_{b,c}$ and $\Delta\xi_{b,c}$ are small, terms in $(\Delta\eta_{b,c})^2$ and $(\Delta\xi_{b,c})^2$ can be neglected when these expressions are substituted into the above equations 26–30 and 31–35. The equations can be written as:

$$n_i'(\mathrm{data}) - \mathrm{n_i'(trial)} \;\; = \;\; \sum_j A_{ij}\Delta_j. \tag{38}$$

where $n_i'(\mathrm{trial})$ is the value of n' predicted with the trial efficiencies, and $n_i'(\mathrm{data})$ is the data value. The shorthand $\Delta_1 = \Delta\eta_b$, $\Delta_2 = \Delta\eta_c$, $\Delta_3 = \Delta\xi_b$ and, $\Delta_4 = \Delta\xi_c$ has been used.

The values of $\Delta\eta_{b,c}$ and $\Delta\xi_{b,c}$ were unfolded using a singular-value decomposition (SVD) technique [18]. A χ^2 with an additional regularisation term was minimised:

$$\min\left\{\sum_{i=1}^{5}\left(\frac{\sum_{j=1}^{4}A_{ij}\Delta_j}{\sigma_i'}\right)^2 + \tau\sum_{k=1}^{4}\Delta_k\Delta_k\right\}, \tag{39}$$

which constrained the length of the vector Δ to be small; i.e. the approximation that the equations were linear is a good one. If the solutions were not small the 'linearising' procedure was not valid, so the trial values were modified and the procedure was repeated, until the solutions were small.

Following the suggestion given in ref. [18] τ was chosen to be $\tau = s_3^2$, where s_3^2 is the third singular value of matrix A. This choice is a compromise between too weak a constraint, resulting in essentially the normal χ^2 fit, and too hard a constraint, in which case the solution $\sum_{k=1}^{4}\Delta_k\Delta_k = 0$ would be forced.

The hemisphere tagging efficiencies η and ξ were found from the unfolded values of $\Delta\eta_{b,c}$ and $\Delta\xi_{b,c}$.

Acknowledgements

We particularly wish to thank the SL Division for the efficient operation of the LEP accelerator and for their continuing close cooperation with our experimental group. In addition to the support staff at our own institutions we are pleased to acknowledge the
Department of Energy, USA,
National Science Foundation, USA,
Particle Physics and Astronomy Research Council, UK,
Natural Sciences and Engineering Research Council, Canada,
Israel Science Foundation, administered by the Israel Academy of Science and Humanities,
Minerva Gesellschaft,
Japanese Ministry of Education, Science and Culture (the Monbusho) and a grant under the Monbusho International Science Research Program,
German Israeli Bi-national Science Foundation (GIF),
Direction des Sciences de la Matière du Commissariat à l'Energie Atomique, France,
Bundesministerium für Bildung, Wissenschaft, Forschung und Technologie, Germany,
National Research Council of Canada,
Hungarian Foundation for Scientific Research, OTKA T-016660, and OTKA F-015089.

References

[1] *Z Physics at LEP 1 - Volume 1*, edited by G. Altarelli, CERN 89-08, 1989.

[2] ALEPH collaboration, D. Buskulic *et al.*, Phys. Lett. **B335** (1994) 99;
DELPHI collaboration, P. Abreu *et al.*, Z. Phys. **C63** (1994) 3.

[3] OPAL collaboration, R. Akers *et al.*, Z. Phys. **C67** (1995) 365.

[4] ALEPH Collaboration, D. Buskulic *et al.*, Phys.Lett. **B384** (1996) 414; DELPHI Collaboration, P. Abreu *et al.*, Z.Phys. **C65** (1995) 569;
L3 Collaboration O. Adriani *et al.*, Phys.Lett. **B292** (1992) 454;
OPAL Collaboration, G. Alexander *et al.*, Z. Phys. **C70** (1996) 357.

[5] DELPHI Collaboration, P. Abreu *et al.*, Z.Phys.**C66** (1995) 341;
OPAL Collaboration, G. Alexander *et al.*, *'A Measurement of the Charm and Bottom Forward-Backward Asymmetries using D Mesons at LEP'*, CERN-PPE/96-101, to be published in Z. Phys. C.

[6] OPAL Collaboration, K. Ahmet *et al.*, Nucl. Instr. and Meth. **A305** (1991) 275;
P. P. Allport *et al.*, Nucl. Instr. and Meth. **A 346** (1994) 476;
P. P. Allport *et al.*, Nucl. Instr. and Meth. **A 324** (1993) 34.

[7] OPAL Collaboration, G. Alexander *et al.*, Z. Phys. **C52** (1991) 175.

[8] JADE Collaboration, Z. Phys. **C33** (1986) 175;
JADE Collaboration, Phys. Lett. **B213** (1988) 235.

[9] OPAL Collaboration, M. Z. Akrawy *et al.*, Z. Phys. **C49** (1991) 375.

[10] T. Sjöstrand, Comp. Phys. Comm. **39** (1986) 347;
T. Sjöstrand and M. Bengtsson, Comp. Phys. Comm. **43** (1987) 367;
T. Sjöstrand, CERN-TH.6488/92.

[11] J. Allison *et al.*, Phys. Rev. **A317** (1992) 47.

[12] OPAL Collaboration, M. Z. Akrawy *et al.*, Z. Phys. **C47** (1990) 505.

[13] OPAL Collaboration, G. Alexander *et al.*, Z. Phys. **C69** (1996) 543.

[14] C. Peterson, D. Schlatter, I. Schmitt, and P. Zerwas, Phys. Rev. **D27** (1983) 105.

[15] G. Marchesini *et al.*, Comp. Phys. Comm. **67** (1992) 465.

[16] OPAL Collaboration, R. Akers *et al.*, Z. Phys. **C65** (1995) 17;
OPAL Collaboration, K. Ackerstaff *et al.*, *An improved measurement of* R_{b} *using a double tagging method*, CERN PPE/96-167, submitted to Z. Phys. C.

[17] OPAL Collaboration, R. Akers *et al.*, Z. Phys. **C66** (1995) 19.

[18] A. Hocker and V. Kartvelishvili, Nucl. Instr. and Meth. **A372** (1996) 469.

[19] D. Bardin *et al.*, CERN-TH-6443/92, May 1992.
The input parameters used were $M_{\mathrm{Z}} = 91.187\,\mathrm{GeV}/c^2$, $M_{\mathrm{Higgs}} = 300\,\mathrm{GeV}/c^2$ and $\alpha_s = 0.121$.

[20] OPAL Collaboration, R. Akers *et al.*, Z. Phys. **C61** (1994) 209.

[21] MARKIII collaboration, D.Coffman *et al.*, Phys. Lett. **B263** (1991) 135.

[22] The LEP collaborations, Nucl. Instr. and Meth. **A378** (1996) 101.

[23] Particle Data Group, R.M. Barnett *et al.*, Phys. Rev. **D54** (1996) 1.

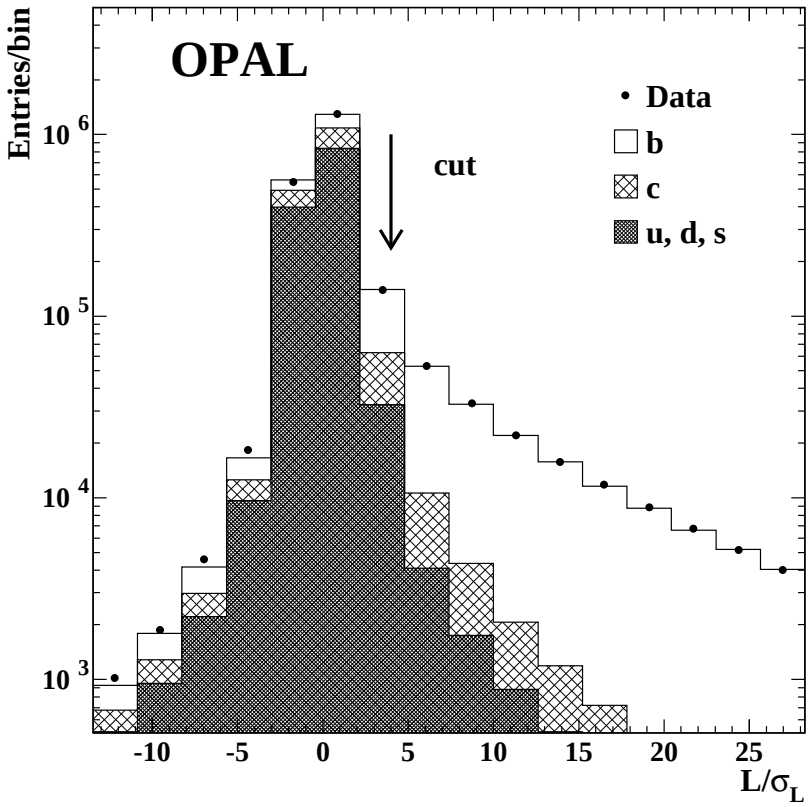

Figure 1: The decay length significance distribution in data and Monte Carlo. Shown are data, the bottom, the charm and the light flavour components.

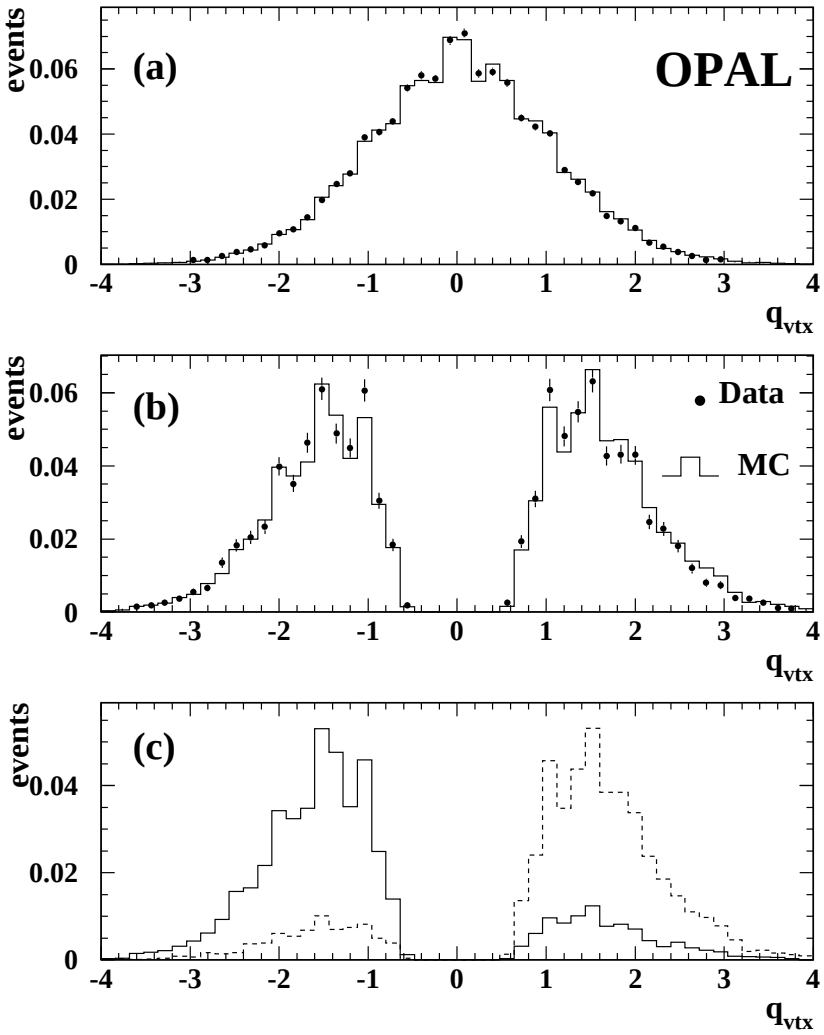

Figure 2: Vertex charge distributions in data and in Monte Carlo (a) before and (b) after the $|q_{\rm vtx}| > 1.4\sigma_q + 0.2$ and neural network cuts. Figure (c) shows the Monte Carlo $q_{\rm vtx}$ distribution split into the positively (dashed line) and negatively (solid line) charged primary quark hemispheres.

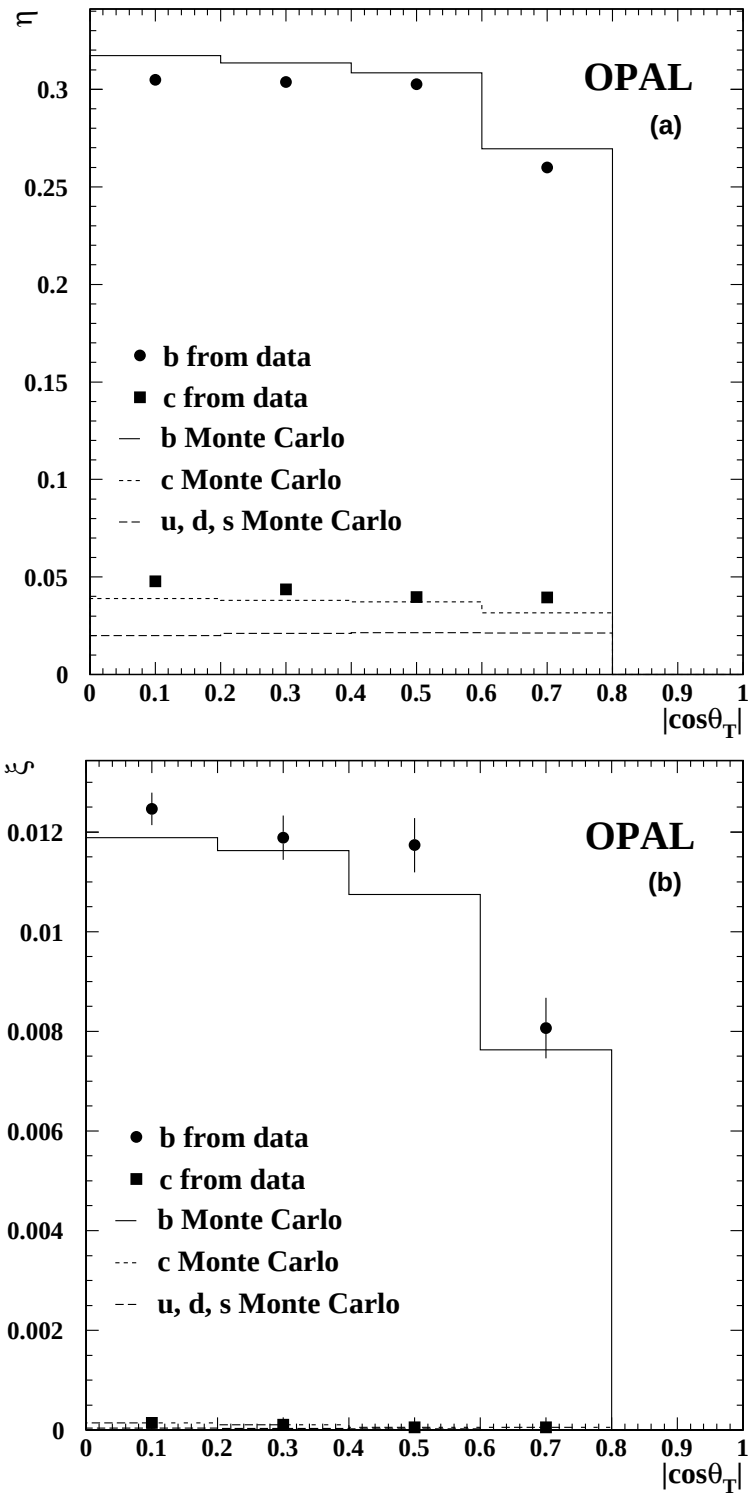

Figure 3: The fitted (a) lifetime tagged hemisphere and (b) $q_{\rm vtx}$ hemisphere tagging efficiencies for each $|\cos\theta_{\rm T}|$ bin. The histograms are the corresponding Monte Carlo quantities. Any discrepancy between the data and Monte Carlo b hemisphere efficiencies has no effect on the measurement as the values obtained from the data were used.

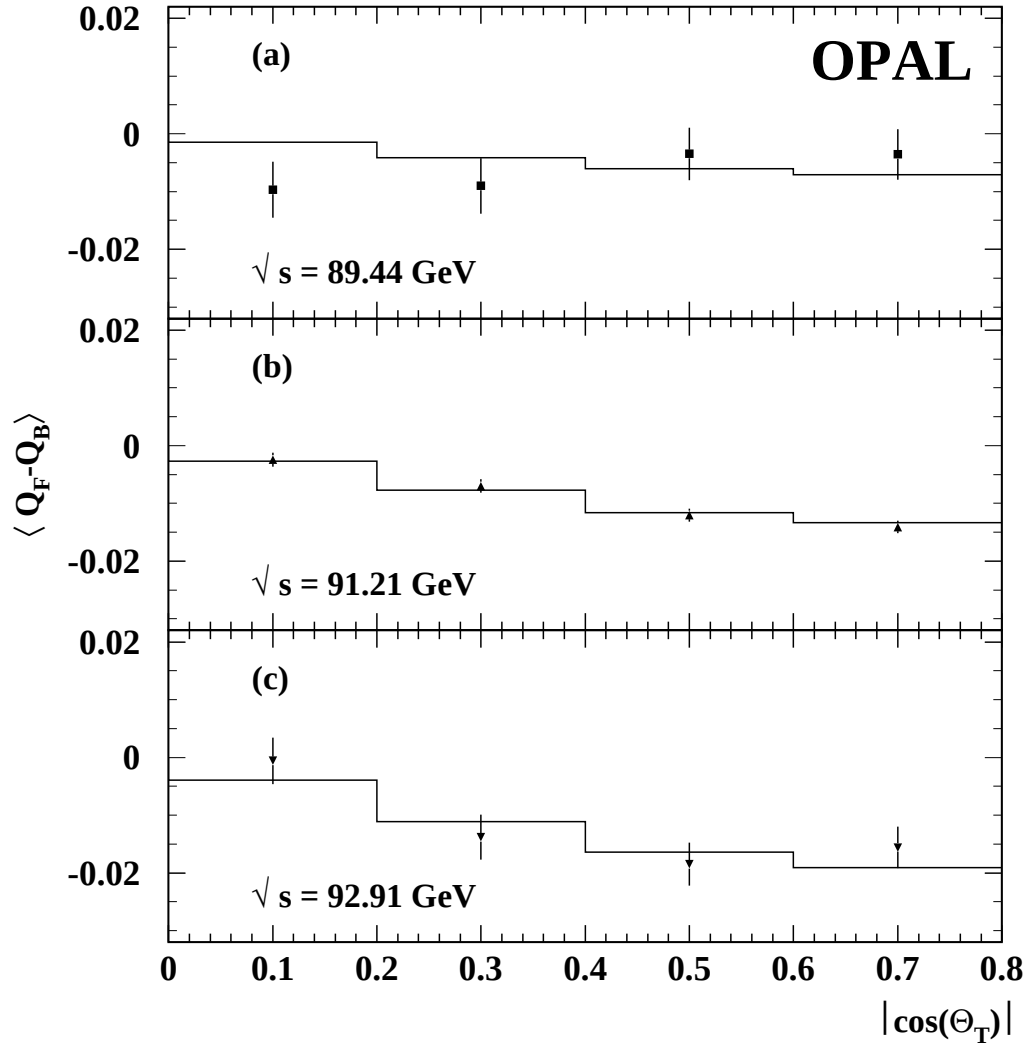

Figure 4: The charge flow as a function of $\cos\theta_{\mathrm{T}}$. Shown are the data (points with error bars) for the three energies (a) peak-2, (b) peak and (c) peak+2, and the results from the measurement presented in this paper for these energy ranges (line histogram). Note that these distributions are not actually used to derive the results, but are only included as an illustration of the results.

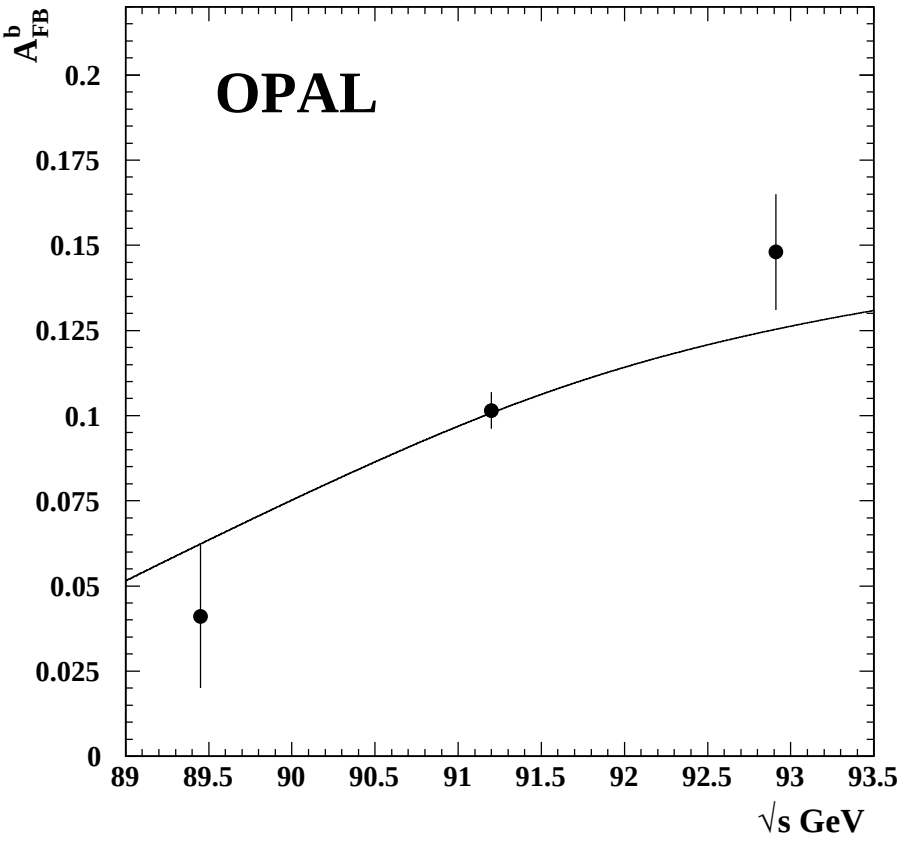

Figure 5: The asymmetry measured using the data collected in 1991-1995 as a function of the centre-of-mass energy. The curve is the Standard Model prediction for $A_{\rm FB}^{\rm b}$ using the fitted value of $\sin^2\theta_{\rm W}^{\rm eff,e}$.